Applied Physics Reviews

RESEARCH ARTICLE | OCTOBER 23 2023

Untethered kirigami soft robots with programmable locomotion

Jinqiang Wang ; Ruichen Wang ; Zixiao Zhu ; Kun Zhou ; Dong Wang

Check for updates

Appl. Phys. Rev. 10, 041405 (2023)
https://doi.org/10.1063/5.0155355

CrossMark

View Online

Export Citation

Articles You May Be Interested In

A functional integral formalism for quantum spin systems

J. Math. Phys. (July 2008)

Modes selection in polymer mixtures undergoing phase separation by photochemical reactions

Chaos (June 1999)

Spreading of a surfactant monolayer on a thin liquid film: Onset and evolution of digitated structures

Chaos (March 1999)

23 October 2023 12:40:25

AIP Advances

Why Publish With Us?

25 DAYS average time to 1st decision

740+ DOWNLOADS average per article

INCLUSIVE scope

Learn More

AIP Publishing

AIP Publishing

Applied Physics Reviews ARTICLE pubs.aip.org/aip/are

Untethered kirigami soft robots with programmable locomotion

Cite as: Appl. Phys. Rev. **10**, 041405 (2023); doi: 10.1063/5.0155355
Submitted: 19 April 2023 · Accepted: 26 September 2023 ·
Published Online: 23 October 2023

View Online Export Citation CrossMark

Jinqiang Wang,[1] Ruichen Wang,[1] Zixiao Zhu,[1] Kun Zhou,[2] and Dong Wang[1,a)]

AFFILIATIONS

[1]State Key Laboratory of Mechanical System and Vibration, School of Mechanical Engineering, Shanghai Jiao Tong University, 800 Dongchuan Road, Shanghai 200240, China
[2]Singapore Centre for 3D Printing, School of Mechanical and Aerospace Engineering, Nanyang Technological University, 50 Nanyang Avenue, Singapore 639798, Singapore

[a)]Author to whom correspondence should be addressed: wang_dong@sjtu.edu.cn

ABSTRACT

Kirigami can induce shape transformations in planar and nonplanar geometry by rational cut design, significantly increasing the kinematics degree of freedom. Here, we exploit kirigami metamaterials and hard-magnetic actuation to design untethered soft robots. The kirigami soft robot, consisting of slit perforated kirigami patterns with embedded hard-magnetic disks in each facet, exhibits modularity, scalability, and programmable locomotion. By varying the magnetization arrays, the kirigami soft robots show diverse static and dynamic behaviors, which are systematically studied by experiments and FEM. We demonstrate multi-module soft robots with programmable locomotion, where directional locomotion is generated by a synergistic effect and circular motion is realized by the asymmetric pattern. Active and passive environmental adaptabilities and multifunctionalities are shown, including passing over gaps, active obstacle avoidance, moving over various substrates, carrying loads, remote circuit switches, and amphibious motions by bistability. This work paves the way to design untethered soft robots with programmable motions and multifunctionalities.

Published under an exclusive license by AIP Publishing. https://doi.org/10.1063/5.0155355

23 October 2023 12:40:25

I. INTRODUCTION

Controllable locomotion is essential to creatures in nature for moving, preying, and fleeing, which is equally desirable in soft robotics. Unlike conventional rigid robots that realize motions by controlling high-power engines and transmission systems, the programmable locomotion of soft robots is based on functional soft materials and structural design.[1–5] Functional soft materials, such as shape memory polymers, dielectric elastomers, and magnetic, responsive materials, provide actuation under light, thermal, magnetic or external stimulations.[6–13] Among them, hard-magnetic soft materials, obtained by embedding hard-magnetic particles (e.g., neodymium–iron–boron alloy, NdFeB) into a soft polymeric matrix (e.g., silicone rubber, gels),[8,14] could provide fast, reversible, and untethered actuation by manipulating the external magnetic field.[15–18] The structural design further improves the embodied intelligence of soft robots that converts actuation to controllable physical motions, with no involvement of controllers or processing units.[19–24]

A widely used method to program the locomotion of magnetic soft robots is to design the magnetization profile. Varying magnetization profiles can generate localized magnetic torques under external magnetic fields, which cause the soft robots' shape deformations. Magnetic soft robots with various shape deformations and multifunctionalities have been developed, such as millimeter soft robots with multimodal locomotion on complex terrains,[25] variable-stiffness robots with reversible actuation and shape locking,[26] integrated multifunctional robots with customized deformation and functions,[27] and 3D-printed untethered robots with auxetic mechanical behaviors and reconfigurable configurations.[28] Computational methods have also been developed to predict the shape change with prescribed magnetization profiles or inversely design the profiles according to desired deformation.[8,29–31] However, this method requires complex magnetization profiles and sophisticated manipulation of the magnetic fields. Achieving accurate magnetization profiles remains challenging due to the non-homogenized magnetic particles, fabrication errors and cumbersome manufacturing processes, although various fabrication techniques have been proposed, such as 3D printing,[28,32] jigs molding,[25,30,33,34] lithography,[35,36] spraying,[37] laser reprogramming,[38,39] roll-to-roll,[27,40] and modular assembly with bonding agents.[21,41] Accurate manipulation of the magnetic fields also requires exquisite equipment and skilled operations.

Published under an exclusive license by AIP Publishing

Another method to realize programmable shape change is using metamaterials, such as origami,[42–45] lattice,[46,47] and heterogeneous 3D frames.[48,49] Metamaterials impart exceptional properties and functionalities that differ from and surpass those of the constituent hard-magnetic soft materials, improving embodied intelligence and mitigating the dependence on accurate magnetization profiles and sophisticated magnetic control. Versatile behaviors, such as bistability, high stretchability, and negative Poisson's ratio, can be realized using metamaterials even with simple magnetization profiles and magnetic fields. For example, the bistability of Kresling origami has been exploited to design robotic arms,[43] spinning robots,[44] and crawlers.[45] Voxelated three-dimensional magnetic soft machines were designed with programmable shape morphing, negative Poisson's ratio, and complex stiffness distribution.[48] Although several metamaterials have been proposed to design untethered soft robots, the development of soft robots with modularity, scalability and programmable locomotion is still limited.

Kirigami, an ancient art of creating beautiful decorations by cutting, involve strategically configured cuts to guide buckling/folding processes by releasing the continuous constraint in the constituent sheet material.[50,51] By rational cut design, kirigami can induce shape transformations in the planar or nonplanar geometry, significantly increasing the kinematics degree of freedom.[52] The kirigami facets provide platforms for embedding functional components, creating opportunities to build the next generations of soft robotics. The periodic arrangements of the kirigami patterns further enable easy combination of modular units. Another unique characteristic of kirigami is scalability, indicating that kirigami soft robots of different sizes follow similar working principles.[53] Therefore, kirigami metamaterials provide a promising way to design modular and scalable soft robots with controllable locomotion.

Here, we develop an untethered kirigami soft robot consisting of slit perforated kirigami patterns with embedded hard-magnetic disks in each facet, which exhibits modularity, scalability and programmable locomotion. The hard-magnetic disks provide localized magnetic actuation, while the kirigami patterns provide large deformation and diverse functions. The deformation and locomotion are studied systematically using experiments and FEM. The periodic kirigami structures further endow the untethered soft robots with modularity and scalability. Multiple modular units are combined to improve the structural and loading capabilities, and kirigami soft robots of different sizes are designed. We demonstrate multi-module soft robots with programmable locomotion, such as walking, crawling, flapping, swimming, and swing locomotion. Direction change is realized by the phase differences of magnetic fields, and asymmetric (AS) pattern enables circular motion. Active and passive environmental adaptabilities and multifunctionalities are shown, including passing over gaps, active obstacle avoidance, moving over various substrates, carrying large items, remote circuit switches, and amphibious motions by bistability. This work paves the way to design untethered soft robots with programmable locomotion and multifunctionalities.

II. DESIGN AND CONTROL OF KIRIGAMI SOFT ROBOTS

A. Structural design

The periodic kirigami pattern is shown in Fig. 1(a). A typical slit perforated pattern is used, formed by orthogonal slit perforations with length l and width δ. The slit perforations divide each kirigami unit into four squares with the ability to rotate around the hinges in-plane and out-of-plane. Single- or multiple-module kirigami soft robots can be designed using the periodic kirigami pattern. Four hard-magnetic disks with identical dimensions (diameter R and thickness t) are embedded into the center of each square with predefined orientations [Fig. 1(b)]. The left and right sides of the soft robots are closed with a straight beam to guarantee stability (Movie 6).

Two methods are used to fabricate the kirigami structures. The kirigami structure can be made from silicone rubber (Smooth-On, Inc., Ecoflex 00–50) by molding [Fig. 1(c)], while digital light processing 3D printing is able to fabricate miniature kirigami structures. The magnetic disks are fabricated by mixing 20 vol. % hard-magnetic particles (neodymium–iron–boron, NdFeB, ∼5 μm in size) into the silicone rubber through a thorough stirring. After being magnetized under an impulse field (∼2 T), the magnetic disks possess an in-plane magnetization $\mathbf{M}$ along the x-axis. When an external field $\mathbf{B}$ is applied, the magnetic unit tends to align its direction with the applied field resulting from the magnetic torque $\mathbf{T} = \mathbf{M} \times \mathbf{B}$, which deforms the kirigami structures simultaneously due to the strong bonding. The kirigami pattern enables large deformation, while the hard-magnetic disks provide localized magnetic torque. In particular, in-plane rotation is exhibited when a y-directional magnetic field is applied, while a z-directional magnetic field enables out-of-plane deformation. In addition, bending and rotation deformation is superimposed under a combined magnetic field $\mathbf{B}_y$ and $\mathbf{B}_z$ [Fig. 1(d)]. The developed kirigami soft robots enable modular combination by virtue of the extensibility of kirigami pattern. Figure 1(e) shows single-module and two-module kirigami soft robots.

A local coordinate (X, Y, Z) is set along the length, width and thickness directions of the kirigami soft robot. We set the orientation of the magnetic disk along the positive or negative X direction for convenience. Depending on the orientations of the four magnetic disks, a single-module kirigami soft robot possesses 16 different patterns (Fig. S2), which can be divided into five categories: (i) symmetric about both the X- and Y-axis (XYS) (ii) symmetric about X-axis only (XS) (iii) symmetric about Y-axis only (YS) (iv) antisymmetric to the center (ANS), and (v) asymmetric (AS) [Fig. 1(f)]. The motions of soft robots in the same category are consistent by merely adjusting the magnetic field. Kirigami soft robots in different categories exhibit diverse deformations and motions by varying the orientation direction and applied magnetic fields [Fig. 1(g)].

B. Static deformation

The kirigami pattern couples with the localized magnetic torque to form diverse deformed shapes in a noncontact manner. We develop a FEM method to predict the static deformation of the kirigami soft robots under various magnetic fields (Fig. S3). Figure 2 shows the experimental and FEM static deformations of the five typical single-module kirigami soft robots when applying y and z magnetic fields. A global coordinate (x, y, z) is used. Magnetic fields along the x, y, and z directions are denoted as $\pm\mathbf{B}_x$, $\pm\mathbf{B}_y$ and $\pm\mathbf{B}_z$, respectively. The symbol "+" and "−" represent magnetic fields with positive or negative directions. Note that the kirigami soft robots show no deformation when an x magnetic field is applied, as the initial magnetization direction X is coincident with the x direction (Figs. S5 and S6).

23 October 2023 12:40:25

Published under an exclusive license by AIP Publishing

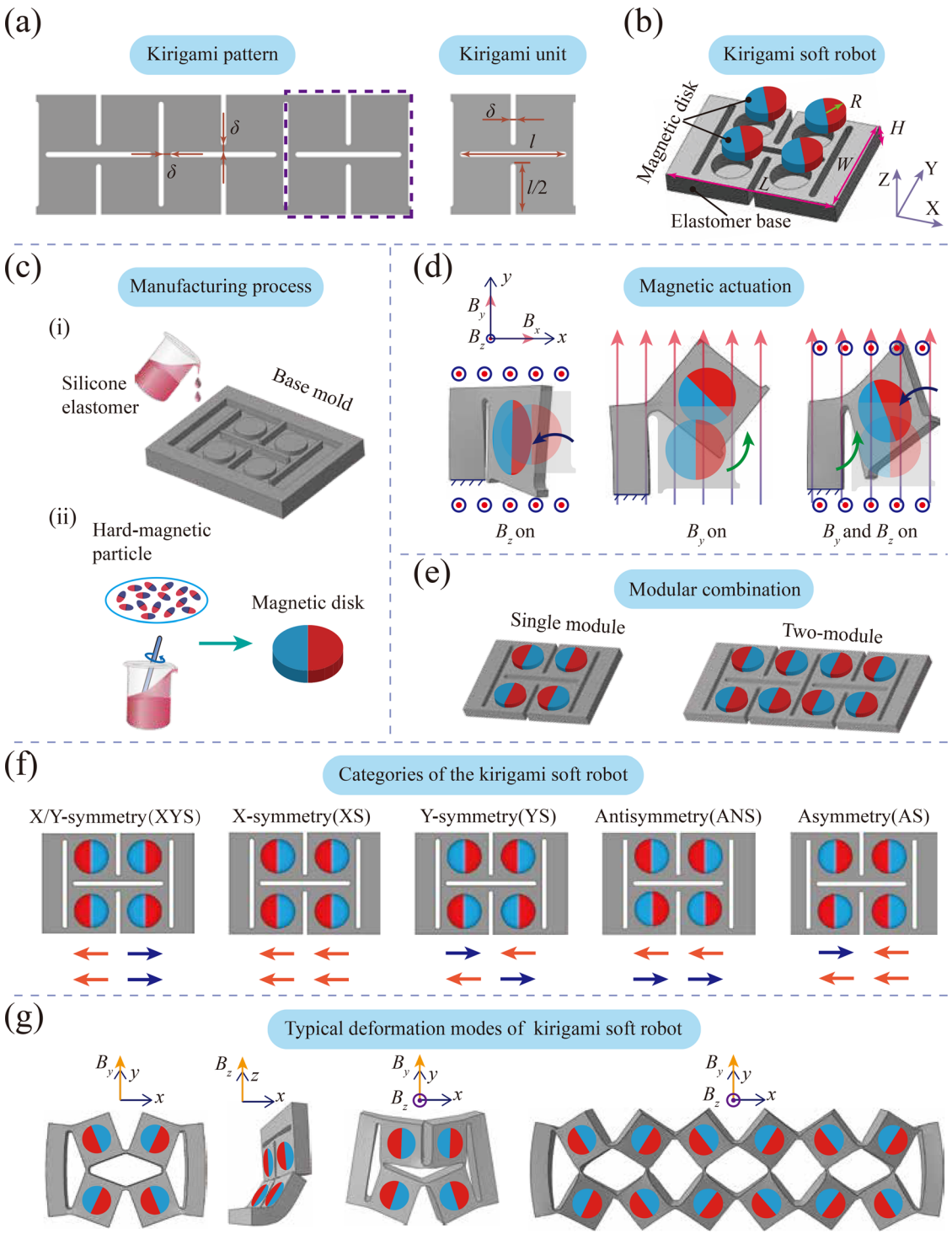

FIG. 1. Structural design of the untethered kirigami soft robots. (a) The kirigami pattern is formed by orthogonal slit perforations with length l and width δ. The periodic pattern enables multi-module combination. (b) The kirigami soft robots are acutated by localized magnetic torque generated from the hard-magnetic disks. (c) Typical manufacturing procedures. (d) The kirigami pattern enables both in-plane and out-of-plane bending. (e) Multi-module soft robots can be designed by combining module units. (f) The kirigami soft robots can be divided into five categories based on the geometries and the magnetization arrays. (g) Typical deformations of the kirigami soft robots under external magnetic fields.

23 October 2023 12:40:25

Published under an exclusive license by AIP Publishing

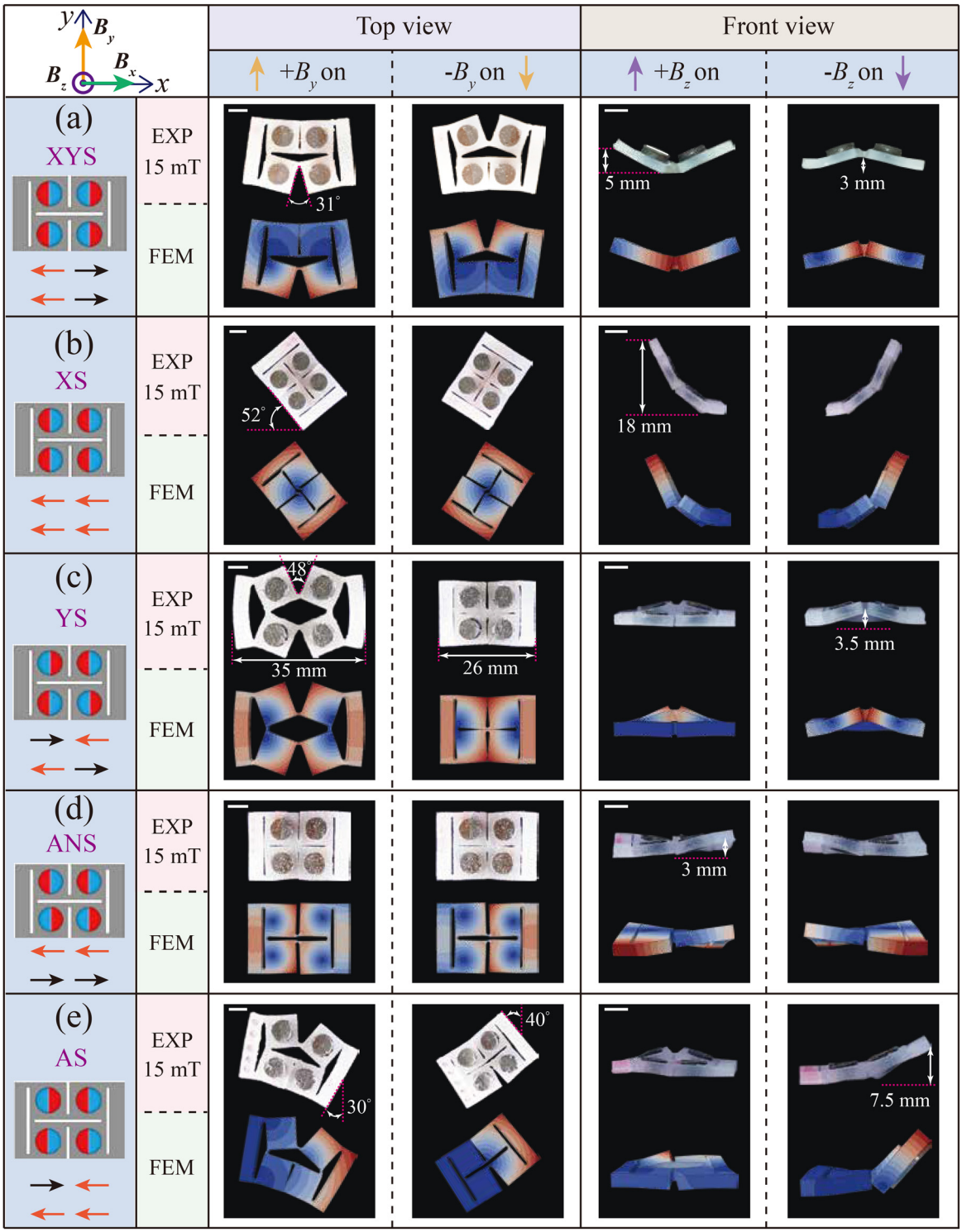

FIG. 2. Static deformation of the kirigami soft robots under $\mathbf{B}_y$ (top view) and $\mathbf{B}_z$ (front view). The kirigami soft robots exhibit diverse in-plane deformation under $\mathbf{B}_y$ and out-of-plane deformation under $\mathbf{B}_z$. The kirigami soft robots are divided into five categories: (a) symmetric about both the X- and Y-axis (XYS), (b) symmetric about X-axis only (XS), (c) symmetric about Y-axis only (YS), (d) antisymmetric to the center (ANS) and (e) asymmetric (AS). The magnitudes of the applied field is 15 mT for all the kirigami soft robots. The corresponding FEM simulated results are given for comparison. All the scale bars are 5 mm.

23 October 2023 12:40:25

Published under an exclusive license by AIP Publishing

1. Magnetic actuation along the y-axis

We can observe that all five kirigami soft robots exhibit in-plane deformations under $\pm\mathbf{B}_y$. The XYS soft robot behaves as a tweezer with the upper and lower halves alternately open and closed. When $+\mathbf{B}_y$ is applied, its left half rotates clockwise while the right half rotates counterclockwise owing to the bilateral symmetric orientations, forming a close upper half and an open lower half. The opening position reverses when $-\mathbf{B}_y$ is applied. The opening angle is around 31° when the magnetic field intensity is 15 mT.

For the XS soft robot, the orientations of the four magnetic disks are the same. Therefore, it shows a rigid body rotation with negligible local deformation. When $+\mathbf{B}_y$ is applied, the same clockwise moments are generated on all four cylinders, generating a clockwise rigid body rotation. Similarly, a counterclockwise rigid body rotation is shown when $-\mathbf{B}_y$ is applied. The rotation angle is around 52° when the magnetic field intensity is 15 mT. As the YS soft robot is symmetry about the Y-axis and asymmetric about the X-axis, the adjacent facets are subjected to magnetic torques in opposite directions. Hence, the adjacent facets rotate around the shared joints in the opposite direction. All the facets rotate away from each other when $+\mathbf{B}_y$ is applied, and the soft robot spreads out. In contrast, all the facets rotate inward when $-\mathbf{B}_y$ is applied. A ∼35% elongation in the x direction with a 48° opening angle along the y-axis is observed when $\mathbf{B}_y = 15$ mT.

No apparent deformation can be observed on the ANS soft robot when $\mathbf{B}_y$ is applied. As the ANS soft robot is antisymmetric about the central point, the magnetic torques on the hinges are counteracted, and all the hinges are locked. Due to the asymmetric magnetization array in the AS soft robot, unbalanced moments are generated. Therefore, the overall deformation consists of a local deformation superimposed on a rigid body rotation. When $+\mathbf{B}_y$ is applied, the torque on the top-left facet is in the counterclockwise direction, while the torques on the other three facets are in the clockwise direction. The AS soft robot rotates clockwise. In addition, the upper part opens as the two upper torques are in the opposite direction, while the lower part closes.

2. Magnetic actuation along z-axis

Unlike the in-plane deformation under $\mathbf{B}_y$, the kirigami soft robots exhibit out-of-plane deformations under $\mathbf{B}_z$. $\mathbf{B}_z$ drives the facets to align their magnetization along the z direction by out-of-plane rotations. Distinct bending configurations are predicted by designing the magnetization array (the last two columns in Fig. 2).

When $+\mathbf{B}_z$ is applied to the XYS kirigami soft robot, moments with $+y$ direction are generated on the left facets and with $-y$ direction on the right facets. The left and right boundaries of the soft robot tend to bend upward, leading to a V-shaped deformation. When $-\mathbf{B}_z$ is applied, the torques' direction is reversed, and the center of the kirigami soft robot pops up. As the magnetic disks' magnetizations are identical in the XS soft robot, it bends as a whole under $\mathbf{B}_z$. Specially, the left part lifts by 18 mm when $\mathbf{B}_z = 15$ mT.

The neighboring facets in the YS soft robot exhibit opposite rotations due to the opposite magnetizations. The front and back halves are raised in an inverted "V" shape and sank in a V shape alternatively under $\pm\mathbf{B}_z$, similar to walking in place. The ANS kirigami soft robot exhibits an antisymmetric deformation, while the AS soft robot shows an asymmetric shape. The top-left facet of the AS soft robot remains on the ground, while the other three facets pop up by about half its body length when $-\mathbf{B}_z = 15$ mT. This asymmetric deformation results in a circular motion when a periodic z magnetic field is applied.

C. Dynamic motions

Multimodal dynamic motions can be generated by taking advantage of the diverse static deformed shapes. Although the deformed shapes are symmetric under a single periodic $\mathbf{B}_y$ or $\mathbf{B}_z$, we demonstrate a synergistic effect when combined $\mathbf{B}_y$ and $\mathbf{B}_z$ are applied due to the structural design, which drives the directional locomotion. The motions of the single-module kirigami soft robots under combined actuation are studied (Movie 1). Periodic square waves with 2 Hz frequency are applied. Zero and π phase differences are used.

Figure 3(a) shows the motion of the XYS kirigami soft robots under combined $\mathbf{B}_y$ and $\mathbf{B}_z$. We first plot the FEM simulated energy evolution in a period. Figure 3(a-ii) plots the potential energy of a XYS kirigami soft robot as the applied magnetic field changes continuously from −15 to 15 mT. Single $\mathbf{B}_y$, $\mathbf{B}_z$, or a combined $\mathbf{B}_y$ and $\mathbf{B}_z$ are used. The potential energy includes the stored strain energy, work done by the magnetic fields and contact, and dissipation due to friction. Note that kinematic energy is not included as the FEM simulation is static. We can observe that the energy is symmetric when a single $\mathbf{B}_y$ or $\mathbf{B}_z$ is applied, indicating symmetric motions in their original position. On the contrary, the energy is asymmetric when a combined field is applied, implying that part of the energy is converted to kinematic energy, which causes directional locomotion. The insight into energy evolution suggests a feasible strategy for programming the locomotion of the kirigami soft robots.

Experiments are then conducted. Results show that the soft robot moves toward the $+y$ direction when the phase difference is 0 and toward the $-y$ direction when the phase difference is π. The directional locomotion results from a synergistic effect when a combined $\mathbf{B}_y$ and $\mathbf{B}_z$ are applied, as a single periodic $\mathbf{B}_y$ or $\mathbf{B}_z$ generates only symmetric motions in its original position (Movie 2). Figure 3(a-iii) shows the trajectory of the bottom center hinge marked by blue dots, and Fig. 3(a-iv) shows experimental and FEM deformed shapes under negative (Mode 1) and positive (Mode 2) $\mathbf{B}_y$ and $\mathbf{B}_z$, respectively. We can observe that the states are the combined states by applying $\mathbf{B}_y$ (alternating tweezer) and $\mathbf{B}_z$ (alternating V shape) separately.

The directional locomotion mechanism is illustrated. When the fields change from negative (Mode 1) to positive (Mode 2), the bottom center hinge drops vertically and immediately. As the fields change from positive (Mode 2) to negative (Mode 1), the two side hinges touch the ground and act as pivots. The XYS kirigami soft robot then moves forward due to the shape change. By applying a periodic oscillating field, the soft robot moves forward continuously. The soft robot moves 50 mm in 9 s, indicating a speed of 5.5 mm/s. The kirigami soft robot moves backward when the phase differences is π with a similar mechanism (Fig. S8). Similarly, the YS kirigami soft robots move toward the $+y$ direction with a speed of 7.4 mm/s when the phase difference is 0 and toward the $-y$ direction when the phase difference is π [Fig. 3(b)].

Another synergetic effect can be observed on the XS kirigami soft robot when a combined $\mathbf{B}_x$ and $\mathbf{B}_z$ magnetic field is applied. Swings in place are observed when a periodic $\mathbf{B}_z$ is applied individually, while no movement shows when applying a periodic $\mathbf{B}_x$ alone. However, when a combined $\mathbf{B}_x$ and $\mathbf{B}_z$ magnetic field is applied, the kirigami soft robot swings in deterministic directions. It swings to the $+x$ direction when

23 October 2023 12:40:25

Published under an exclusive license by AIP Publishing

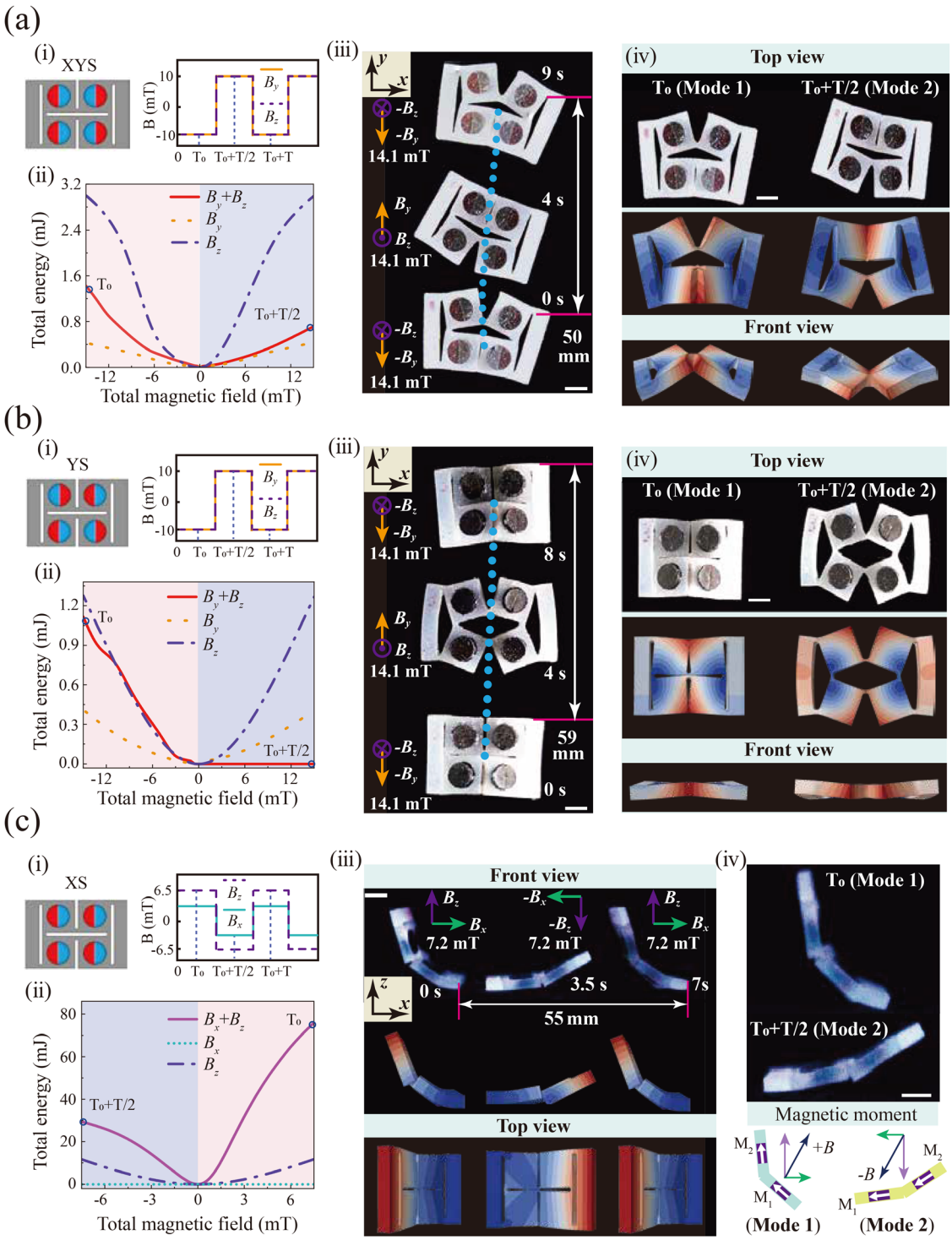

FIG. 3. Dynamic locomotion of the kirigami soft robots. (a) and (b) shows the directional locomotion of the XYS and YS kirigami soft robot under combined $\mathbf{B}_y$ and $\mathbf{B}_z$. (c) shows the swing motion of a XS kirigami soft robot under combined $\mathbf{B}_x$ and $\mathbf{B}_z$. Magnetic fields with periodic square wave at a frequency of 2 Hz are used. (i) shows the applied magnetic fields. (ii) shows that the FEM simulated energy evolutions under single or combined magnetic fields. The asymmetric energy under combined magnetic fields indicates that a synergistic effect is generated. (iii) and (iv) show the locomotion and deformation of the soft robots at various times. The FEM simulated results are given for comparison. All the scale bars are 5 mm.

23 October 2023 12:40:25

Published under an exclusive license by AIP Publishing

the phase difference is 0 [Fig. 3(c)] and to the $-x$ direction when the phase difference is π [Fig. S8(c)]. The moving speed is 7.9 mm/s under a square-wave magnetic field with an intensity of 7.2 mT and a frequency of 2 Hz.

Figure 3(c-ii) plots the energy evolution under various magnetic fields. The dependence of the energy on the magnetic field is symmetric when $\mathbf{B}_x$ or $\mathbf{B}_z$ is applied alone, while it is asymmetric when combined $\mathbf{B}_x$ and $\mathbf{B}_z$ are applied. The energy difference leads to the directional swing in Fig. 3(c-iii). Figure 3(c-iv) shows the swing mechanisms. When positive $\mathbf{B}_x$ and $\mathbf{B}_z$ are applied, moments are generated on the cylinder disks, which lifts the left side of the soft robots (Mode 1). In contrast, the right side is lifted (Mode 2) when a negative $\mathbf{B}_x$ and $\mathbf{B}_z$ is applied. We can observe clearly that the angle between the magnetization and the magnetic field direction in Mode 1 is more significant than in Mode 2, implying a larger moment in Mode 1, which causes the jumping toward the $+x$ direction. The mechanism of moving left when the phase difference is π can be illustrated similarly.

D. Application prospects

The kirigami patterns and the untethered localized magnetic torque enable the dexterous and diverse motions of the kirigami soft robots, showing promising application prospects. The periodic kirigami patterns enable the soft robots' modular combination, which could provide structural and capacity advantages. Another unique characteristic of kirigami is scalability. Kirigami soft robots of different sizes follow similar working principles. The orientation change of the kirigami soft robots leads to distinct motions, which provide active adaptability when navigating in unstructured environments. We also demonstrate multifunctionalities such as carrying loads, remote switches, removing obstacles, circular locomotion and multimodal motions by bistability.

1. Modularity and scalability

The periodic kirigami pattern enables the modular combination of the soft robot. Multi-modular soft robots can be fabricated by repeating the kirigami patterns, which can enhance the robustness of kirigami soft robots in different working scenarios and fulfill unachievable tasks for a single-module soft robot, such as larger output force and more stable locomotion. Figures 4(a-i) and 4(a-ii) exhibit single-, two-, and three-module YS kirigami soft robots under $\pm\mathbf{B}_y$. All the three kirigami soft robots show expansion or contraction deformations.

Figure 4(a-iii) shows the expansion and contraction of single-module YS kirigami soft robots with three different sizes ($L = 14$, 26, and 53 mm). We can observe that the three kirigami soft robots are scalable and follow the same deformation principles (Movie 3). The two larger soft robots are fabricated using molding, while the matrix of the smallest one is 3D printed. Therefore, the design framework of the kirigami soft robot is not confined to specific manufacturing methods or particular feature sizes. Such scalability opens up a broad appeal in environments with different scales, such as in medical or industrial settings.

Figure 4(b) shows XYS kirigami soft robots pushing a large cylinder (diameter is 30 mm, weight is 3.5 g) under a combined periodic $\mathbf{B}_y$ and $\mathbf{B}_z$. The FEM-simulated deformed shapes are shown in Figs. 4(b-i) and 4(b-ii). The cylinder hardly moves as the output force of the single-module soft robot is small [Fig. 4(b-iii)]. By combining two XYS modules, the output force is significantly improved, and the cylinder is moved fast and steady [Fig. 4(b-iv)]. In addition to the output force, the multi-modular soft robots also exhibit structural advantages. For example, Figs. 4(c) and 4(d) show single- and three-module soft robots cross gaps. YS magnetization pattern is chosen. A combined periodic $\mathbf{B}_y$ and $\mathbf{B}_z$ is used. The single-module soft robot can move over a narrow gap (~9 mm). In contrast, the three-module soft robot can cross a bridge with a larger gap up to a module's body length (~20 mm). Therefore, we can use the periodic kirigami structure to modularly combine magnetic soft robots with improved mechanical performances.

2. Active and passive environmental adaptability

The kirigami design improves the embodied intelligence of the soft robots, providing superior active and passive environmental adaptabilities. The kirigami soft robots' locomotion depends on the angle between the magnetization and the applied magnetic field, which may change during motion. The angle change then leads to locomotion behavior change, even under an unchanged magnetic field. This property could provide active adaptability in unstructured environments, which is rarely found in existing soft robots.

We take a two-module XYS kirigami soft robot with different magnetic content as an example. The magnetic content of the cylinder disks of the left module is 20 vol. %, while that of the right module is 10 vol. % [Fig. 5(a-i)]. We first study the locomotion under a periodic magnetic actuation $\mathbf{B}_z$. Both FEM [Fig. 5(a-ii)] and experiments [Fig. 5(a-iii)] show that the soft robot exhibits an alternating M and W shape. The non-homogeneous magnetic contents lead to directional locomotion. When $\mathbf{B}_z$ is positive, the left side bends higher due to the large magnetic contents. Therefore, a large elastic energy is stored in the left part. When $\mathbf{B}_z$ is reversed, the stored elastic energy is released, and the kirigami soft robots crawl toward the right. The locomotion behavior of the soft robot under $\mathbf{B}_y$ alone is investigated next [Fig. 5(b)]. As the left module's magnetic content is larger, the left module expands more than the right module. The non-homogeneous deformation breaks the symmetric and drives the soft robot to rotate anticlockwise (Movie 4).

The different locomotion modes under $\mathbf{B}_y$ or $\mathbf{B}_z$ can be used in active obstacle avoidance [Fig. 5(c)]. A combined $\mathbf{B}_y$ and $\mathbf{B}_z$ with the same phase is applied. When the soft robot encounters a cylindrical obstacle, it rotates around the obstacle with an anticlockwise rotation [similar to the behaviors in Fig. 5(b)]. During the rotation, the soft robot's orientation changes, which induces behavior change. When the rotation angle is 90°, the soft robot crawls forward [similar to the behaviors in Fig. 5(a-iii)] and the soft robot moves away from the obstacle instead of keeping rotating around the cylinder. Note that the external magnetic field remains the same during the whole process. The change in locomotion behaviors results from the orientation change in motion, which is a type of active environmental adaptability.

The kirigami soft robots also exhibit strong passive environmental adaptability. Figure 5(d) shows a two-module YS soft robot moving over various substrates and climbing on a slope. A combined $\mathbf{B}_y$ or $\mathbf{B}_z$ with the same phase is applied, which drives the soft robot to move toward the $+y$ direction. Four substrates are tested: plastic bubble wrap, TPU-coated cotton fabric, spandex fabric and sanding paper [Fig. 5(d-iii)]. The moving speeds are 11.0, 10.2, 10.2, and 10.1 mm/s, respectively. It shows that the soft robots can adapt to various

23 October 2023 12:40:25

Published under an exclusive license by AIP Publishing

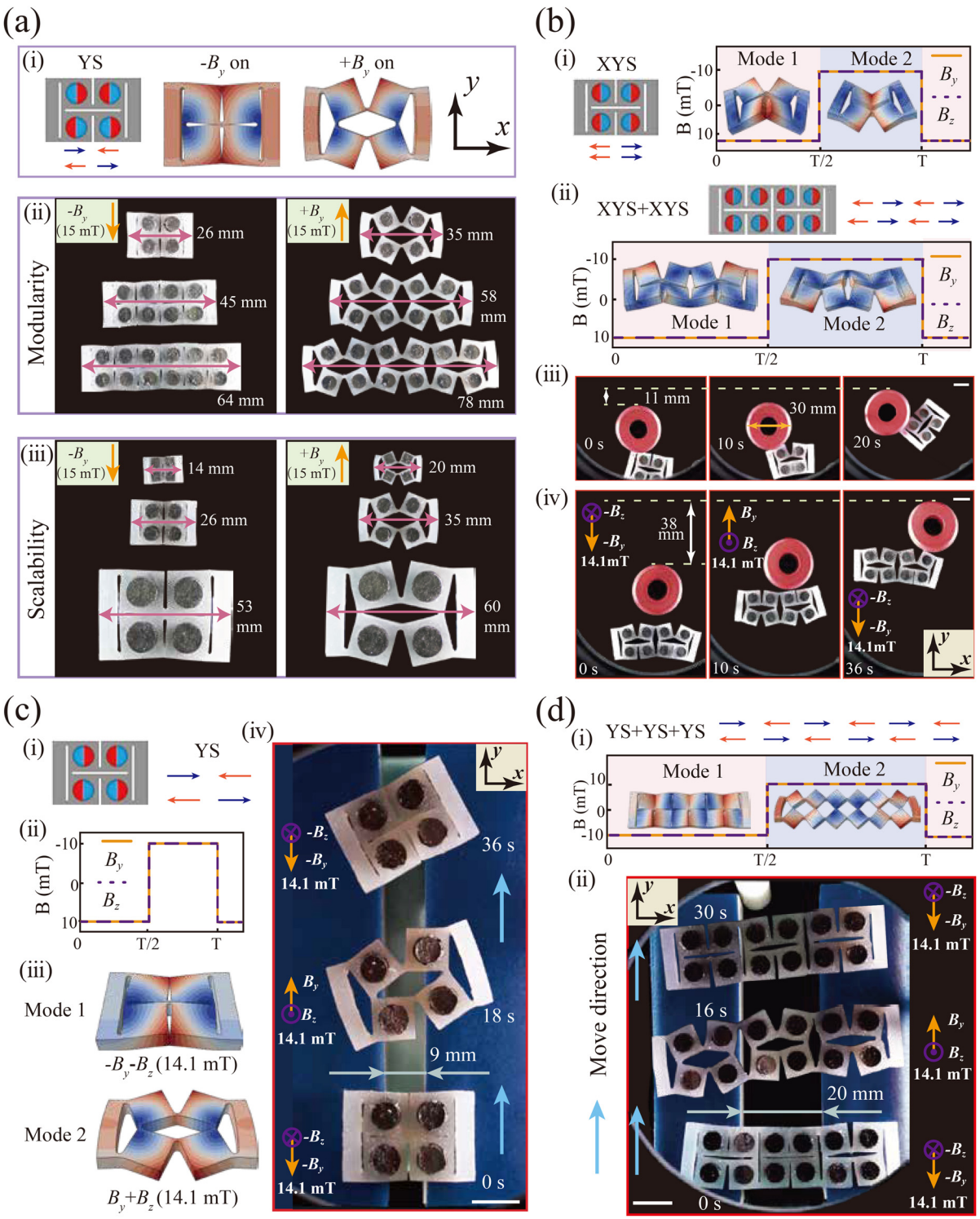

FIG. 4. Modularity and scalability of the soft robots. (a) show the modularity and scalability of the kirigami soft robots. YS modules are used. (b) The multi-module soft robot exhibits a larger output force. A single-module XYS soft robot cannot move a large cylinder. By combining two XYS modules, the output force is significantly improved and the cylinder is moved fast and steady. (c) and (d) A single-module YS kirigami soft robot can move over a gap of 9 mm, while a three-module YS kirigami soft robot can move along two bridges with a larger gap of 20 mm. The FEM simulated deformations are given. All the scale bars are 10 mm.

23 October 2023 12:40:25

Published under an exclusive license by AIP Publishing

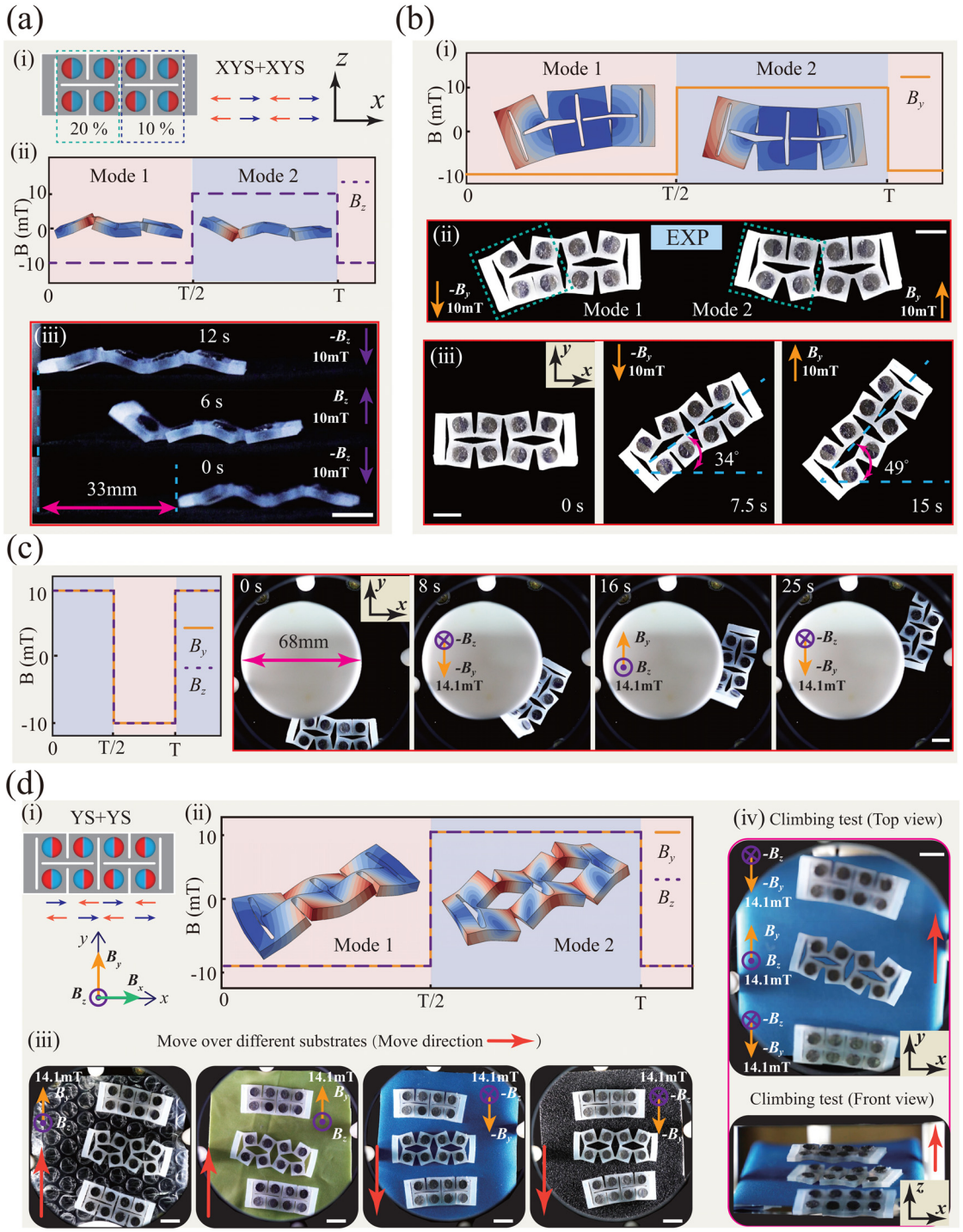

FIG. 5. Active and passive environmental adaptability. (a) A two-module XYS kirigami soft robot is constructed with different magnetic contents (the left is 20 vol. % and the right is 10 vol. %) (i). When applied with a periodic magnetic actuation $\mathbf{B}_z$ (ii), the robot shows alternating M and W shapes, leading to the crawling (iii). (b) When applied with a periodic magnetic actuation $\mathbf{B}_y$, the robot shows an anticlockwise rotation. (c) Under a combined $\mathbf{B}_y$ and $\mathbf{B}_z$ magnetic actuation, the non-homogeneous two-module XYS kirigami robot actively adapt to the obstacle. (d) and (e) The two-module YS kirigami robots show superior passive environmental adaptability, such as moving over various substrates and climbing on a slope with an angle of 17°. The FEM simulated deformations are given for comparison. All the scale bars are 10 mm.

23 October 2023 12:40:25

Published under an exclusive license by AIP Publishing

substrates without much decrease in speed. Climbing slope tests are also conducted. The climbing speed is 4 mm/s when the slope angle is 17° [Fig. 5(d-iv)] (Movie 4).

3. Loading carrying and remote circuit

We demonstrate multi-module kirigami soft robots with the ability to carry a large object, act as a remote circuit switch and remove obstacles on a slope.

As already mentioned in Figs. 2(c) and 4(c), the YS soft robot can form V and inverted V shapes, which is suitable for carrying large objects. Figure 6(a) shows that a two-module YS soft robot can carry a large lattice and move at a speed of 6 mm/s. Load capacity is critical for soft robots to perform transportation in unstructured environment. In addition, a simple circuit is designed in Fig. 6(b). The XS kirigami soft robot behaves as a remote circuit switch by virtue of its large out-of-plane bending deformation. A conductive wire is attached to the right side of the soft robot. The soft robot stays on the ground initially, and bends and connects the circuit when a negative $\mathbf{B}_z$ is applied. The LED device is thus lit on (Movie 5). The robots' ability to remotely control the large deformation facilitates the connection or repair of circuits in limited spaces.

In addition, multiple modules with different types can be combined to achieve coupled motion. For instance, a two-module soft robot composed of XYS and YS modules is designed [Fig. 6(c)]. The two-module soft robot moves from the left-bottom to the right-top corner under a combined $\mathbf{B}_y$ and $\mathbf{B}_z$. As shown in Figs. 3(a) and 3(b), both XYS and YS modules move forward under combined $\mathbf{B}_y$ and $\mathbf{B}_z$. The out-of-plane deflection in XYS module is larger than that in YS module, which drives the two-module soft robot to move in the right

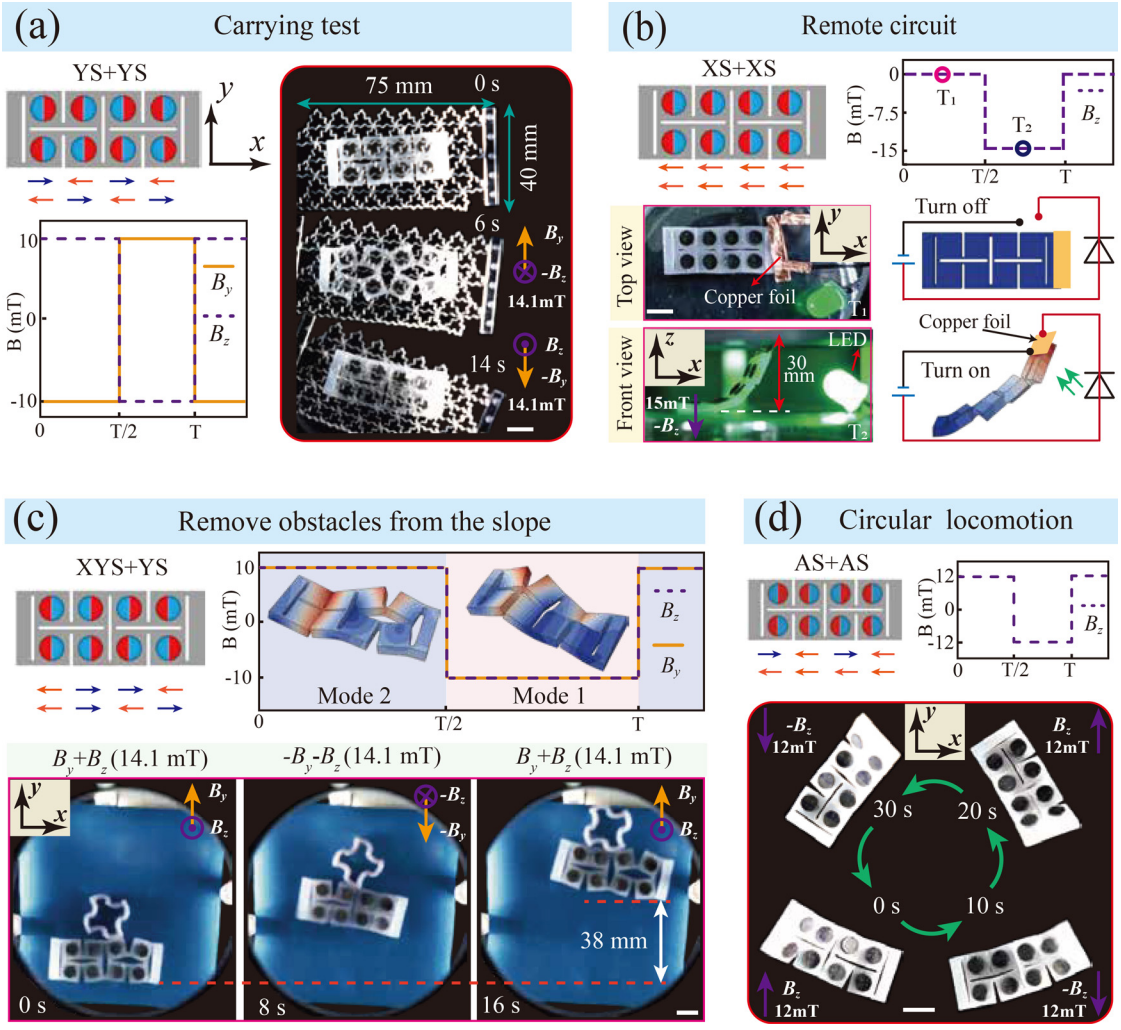

FIG. 6. Multifunctionalities of the kirigami soft robot. (a) A two-module YS soft robot can carry a large lattice and move at a speed of 6 mm/s. (b) The bending deformation of a two-module XS kirigami soft robot can be employed as a remote circuit switch, which lights a LED device upon $-\mathbf{B}_z = 15$ mT. (c) Remove obstacles from the slope. A XYS-YS two-module soft robot can climb and remove a stellate obstacle on a slope with an angle of 10°. (d) A two-module AS soft robot shows a circular motion under a periodic $\mathbf{B}_z$. All the scale bars are 10 mm.

23 October 2023 12:40:25

Published under an exclusive license by AIP Publishing

direction. Therefore, the two-module soft robot moves in the front and right direction simultaneously. In addition to directional motion, the two-module soft robots also possess large force output capability. A stellate obstacle is removed by the soft robot when moving on a slope of 10°.

4. Circular motion

Circular locomotion is challenging for magnetic-driven soft robots, as the orientation of the soft robots changes with the locomotion, which may change the applied torque. Therefore, sophisticated magnetic field control is generally required. The AS module shows an eccentric flapping under $\mathbf{B}_z$ by virtue of the asymmetric magnetization array, which forms a local forward and lateral driving force. Here, a two-module AS soft robot is demonstrated with circular locomotion. $\mathbf{B}_z$ with an intensity of 15 mT and a frequency of 2 Hz is used. The soft robot shows a circular motion with a radius of 25 mm in Fig. 6(d). As $\mathbf{B}_z$ is always perpendicular to the magnetization array, the local forward and lateral driving force does not change with the soft robot's motions. Using the kirigami design, sophisticated magnetic field control is avoided to achieve a 360° turning.

We have designed a single-module YS kirigami soft robot that can move along a closed path using circular and straight motions (Movie 9). The YS kirigami soft robot can realize stable locomotion along straight lines under a combined $\mathbf{B}_y$ and $\mathbf{B}_z$. The magnetization orientation of the disks is shown in Fig. 7(a). The orientation angle is not zero. Therefore, the net magnetization of the four disks is not zero, which enables easy rotation.

The YS kirigami soft robot first moves toward the positive y-axis under a combined $\mathbf{B}_y$ and $\mathbf{B}_z$. The soft robot rotates 90° clockwise when a single $\mathbf{B}_x$ is applied due to the non-zero combined magnetization. After this, the robot moves along the positive x-axis under a combined $\mathbf{B}_z$ and $\mathbf{B}_x$. Subsequently, a $-\mathbf{B}_y$ is applied, and the robot clockwise rotates 90°. The robot moves toward the negative y-axis upon a combined $-\mathbf{B}_y$ and $-\mathbf{B}_z$. After that, the soft robot rotates 90° counterclockwise again under a $\mathbf{B}_x$. Finally, the robot moves along the negative x-axis under a combined $-\mathbf{B}_x$ and $\mathbf{B}_z$ until it returns to the starting point. The soft robot can rotate to any angle by applying a combined $\mathbf{B}_x$ and $\mathbf{B}_y$.

5. Amphibious soft robots by bistability

The kirigami soft robot may exhibit bistability by rationally choosing the geometric parameters and magnetization directions. Here we demonstrate that the bistability of the kirigami soft robot can be employed for mode change. When a positive $\mathbf{B}_x$ magnetic field is applied, the magnetic disks of a YS kirigami soft robot rotates around the hinges, and the kirigami structure transits to another stable state [Figs. 8(a) and 8(b)]. Using the bistability property, we have designed an amphibious soft robot. A lighter EVA (ethylene vinyl acetate) material is used for the base of soft robots, and it can float on the water. Two paddles are attached below the two left magnetic disks. As shown in Fig. 8(c), the kirigami soft robot moves from the ground to the water environment under a combined square-wave $\mathbf{B}_x$ and $\mathbf{B}_z$ magnetic field. When the soft robot enters the pool, a positive $\mathbf{B}_x$ magnetic field is applied, and the kirigami structure transits to another stable state. The paddles also rotate to the suitable position along with the rotation of the magnetic disks. When a combined square-wave $\mathbf{B}_y$ and $\mathbf{B}_z$ superimposed on the constant $\mathbf{B}_x$, the two paddles alternative sink and drive the kirigami soft robot to swim. The kirigami soft robot swims toward the $+y$ direction when the phase difference between $\mathbf{B}_y$ and $\mathbf{B}_z$ is 0, while it swims toward the $-y$ direction when the phase difference is π.

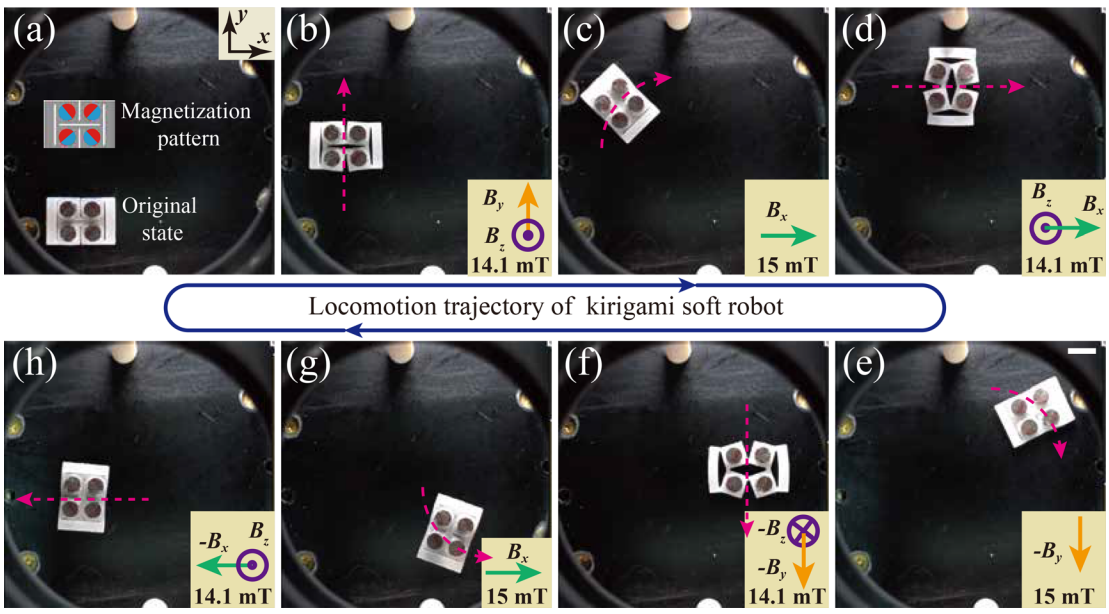

FIG. 7. The YS soft robot can move along a closed path using circular and straight motions. The soft robot moves straightly from the original position (a) to position (b), and then clockwise rotates at position (c), following a straight movement (d) and a clockwise rotation (e), and it continues to move straightly (f) and then counterclockwise rotates at position (g). Finally, it returns to the starting point with a straight movement (h). The scale bar is 10 mm.

23 October 2023 12:40:25

Published under an exclusive license by AIP Publishing

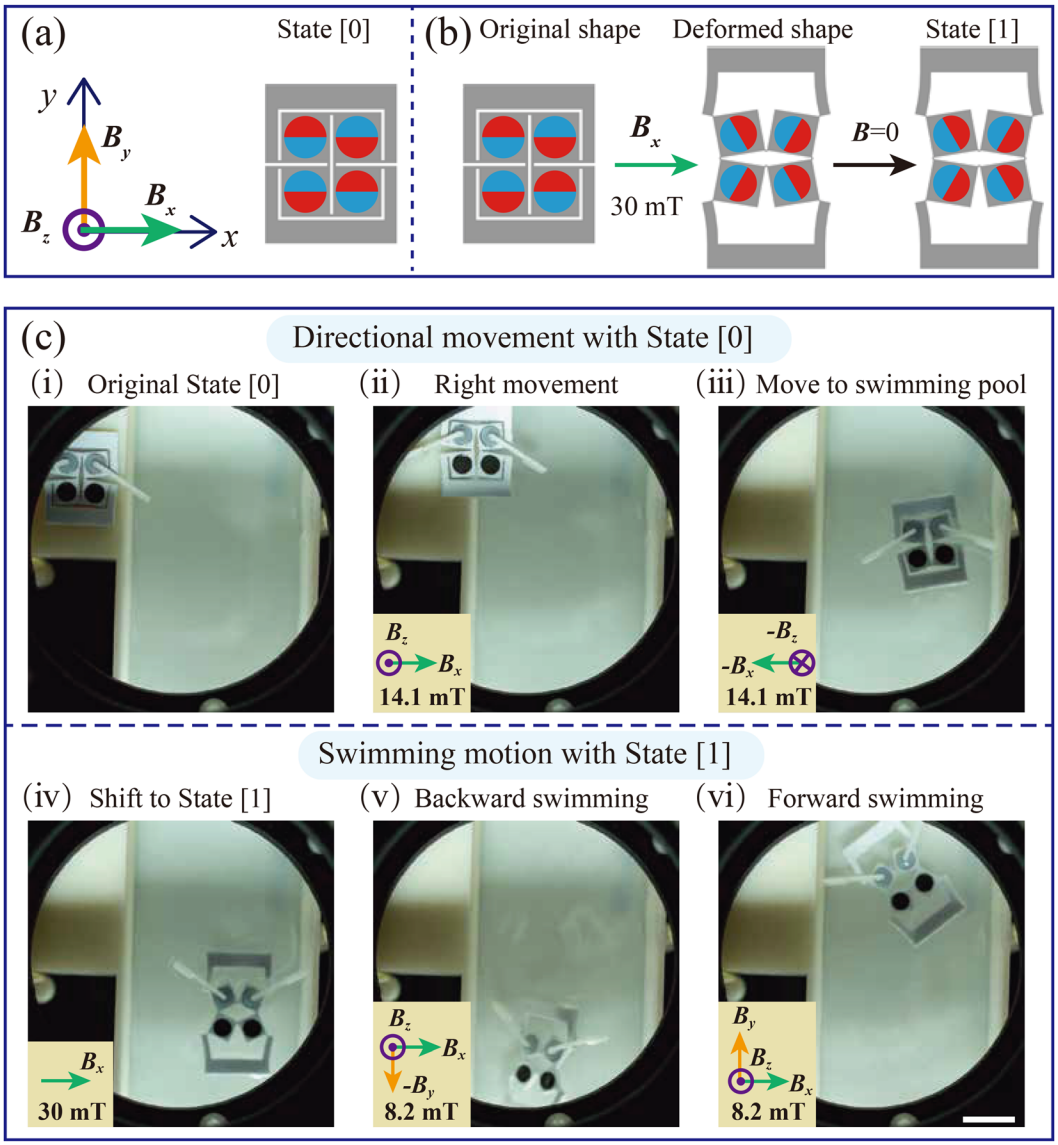

FIG. 8. Amphibious soft robots by bistability. (a) Design of the kirigami soft robot. (b) The soft robot transits to another stable state under a $\mathbf{B}_x$. (c) The locomotion and swimming motion of a bistable YS kirigami soft robot under combined magnetic actuation of $\mathbf{B}_x$, $\mathbf{B}_y$, and $\mathbf{B}_z$. The scale bar is 10 mm.

The detailed magnitudes and directions of the applied magnetic fields are shown in the Movie 7.

6. Swimming and rolling locomotion

The kirigami soft robot can exhibit non-planar locomotion, such as swimming and rolling motions. From the front view of Fig. 2(a), the XYS kirigami soft robot exhibits a non-planar deformation. We have exploited this non-planar deformation for swimming motions (Movie 7). Figure 9 shows the motion of a XYS kirigami soft robot with two thin wings attached to both ends under a square-wave magnetic field $\mathbf{B}_z$. The wings are made from PET films. We can observe that the kirigami soft robot can swim upward along the z direction. The XS soft robot shows rolling locomotion by applying a combined $\mathbf{B}_x$ and $\mathbf{B}_z$ (Fig. S10 and Movie 11).

7. Interaction between soft robots

The interaction between robots is complex but critical for controlling programmable locomotion. We have conducted interaction experiments for the kirigami soft robots (Fig. 10 and Movie 8). As shown in Fig. 10(a), two kirigami soft robots with XS and YS are placed in the workspace. Under a combined $\mathbf{B}_y$ and $\mathbf{B}_z$ square wave magnetic field, the horizontally placed YS soft robot moves in the right direction while the vertically placed XS soft robot rolls. We can observe that the XS soft robot rolls over the YS soft robots. Next, the

23 October 2023 12:40:25

Published under an exclusive license by AIP Publishing

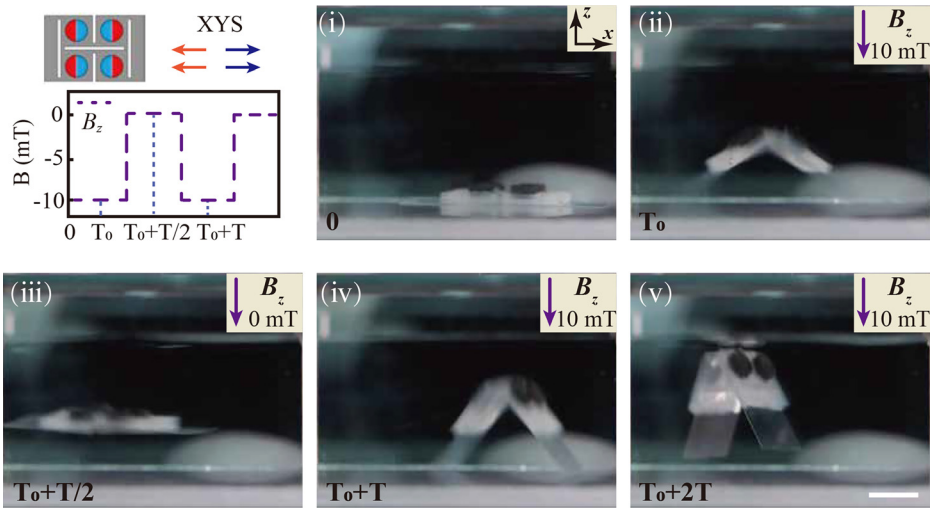

FIG. 9. Swimming motion along *z*-axis of a XYS kirigami soft robots under a square-wave magnetic field $\mathbf{B}_z$. Two thin wings made from PET film are attached at both ends of the robot. The scale bar is 10 mm.

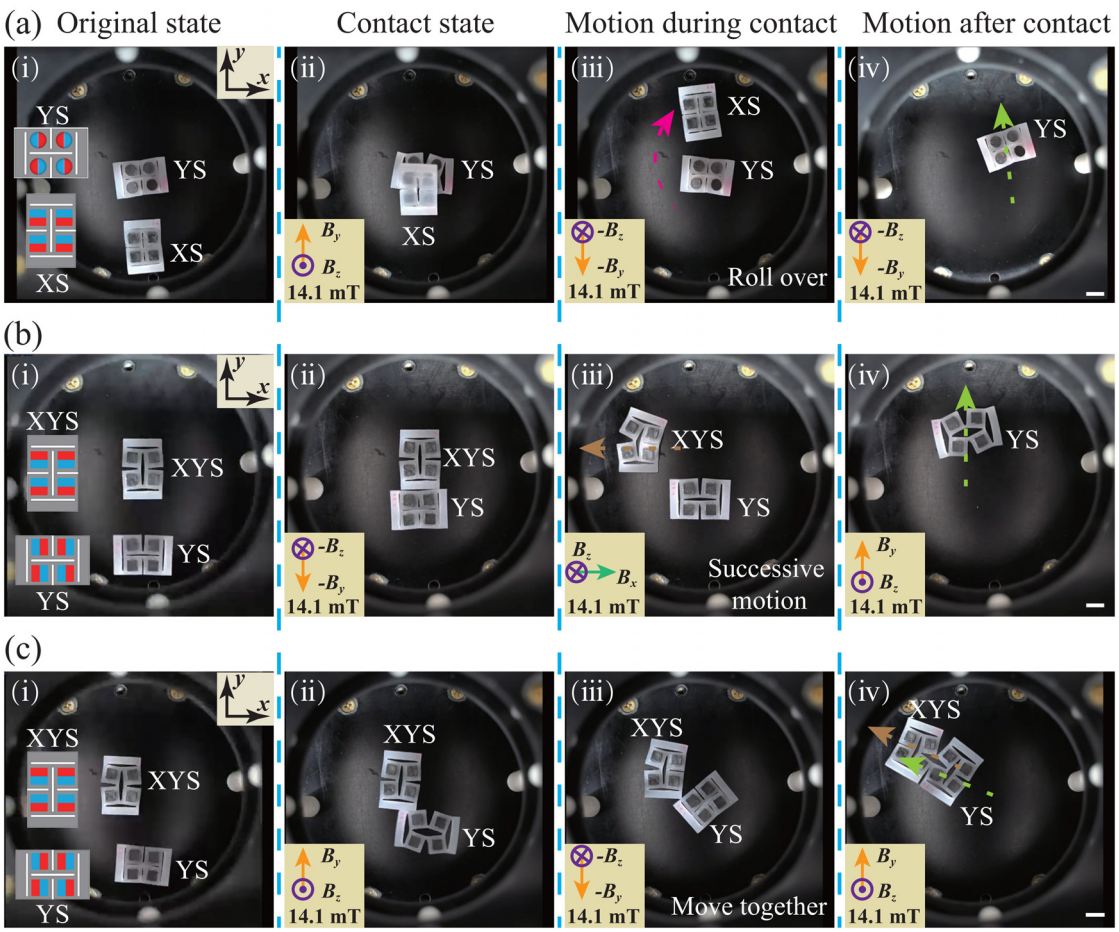

FIG. 10. The interactions between two kirigami soft robots. (a) The interaction between XS and YS soft robots by rolling over. The interaction of XYS and YS soft robots from (b) center and (c) corner directions. All the scale bars are 10 mm.

23 October 2023 12:40:25

Published under an exclusive license by AIP Publishing

interaction between XYS and YS soft robots is studied. When a combined $\mathbf{B}_y$ and $\mathbf{B}_z$ square wave magnetic field is applied, the horizontally placed YS soft robot moves toward the $+y$ direction, while the vertically placed XYS soft robot remains at its initial position [Fig. 10(b-i)]. When the two soft robots contact at the workspace's center, the YS soft robot almost stops [Fig. 10(b-ii)]. When a combined $\mathbf{B}_x$ and $\mathbf{B}_z$ square wave magnetic field is applied, the XYS soft robot can move in the $-x$ direction [Fig. 10(b-iii)]. After that, the YS soft robot continues to move in the $+y$ direction when the magnetic field shifts to a combined square-wave $\mathbf{B}_y$ and $\mathbf{B}_z$ [Fig. 10(b-iv)]. If the YS soft robot contacts the XYS soft robot from the left-bottom corner, the interaction force will change the orientation of both soft robots [Fig. 10(c)]. The YS soft robot will then move due to the change in the magnetization orientations. Hence, both soft robots will move toward the right-top direction.

8. Kirigami soft robots with different cutting patterns

Kirigami offers an incredibly diverse range of patterns due to the infinite possibilities of various cuts and provides promising functions. Here we explore the behaviors of soft robots with other types of kirigami patterns (Movie 10). The cutting pattern in Fig. 11(a) is based on motifs found in the twin tomb towers located in western Iran.[54] It contains four square plates, each connected by four hinges. The location and magnetization directions of the magnetic disks are shown. The applied magnetic field is shown in the second column. The experimental snapshots demonstrate that the soft robot moves toward the $+y$ direction.

Another kirigami pattern is the triangular kirigami, which contains six triangular plates [Fig. 11(b)]. Hinges link the adjacent plates. All the magnetization directions are set along the positive or negative x direction. When a $\mathbf{B}_y$ magnetic field is applied, each triangular plane forms a clockwise/counterclockwise rotation around the hinges, which shows an alternative expansion and contraction with large volume change. We have also varied the aspect ratio of the simple slit perforation kirigami pattern [Fig. 11(c)]. The XS kirigami pattern is used. The experimental snapshots demonstrate that the soft robot moves toward the $+y$ direction under a combined $\mathbf{B}_y$ and $\mathbf{B}_z$, similar to the normal XS kirigami soft robot.

III. DISCUSSION

A. Geometry of the magnetic units

To ensure the alignment of the magnetization direction, we draw a mark on the magnetic disk before magnetization. After magnetization,

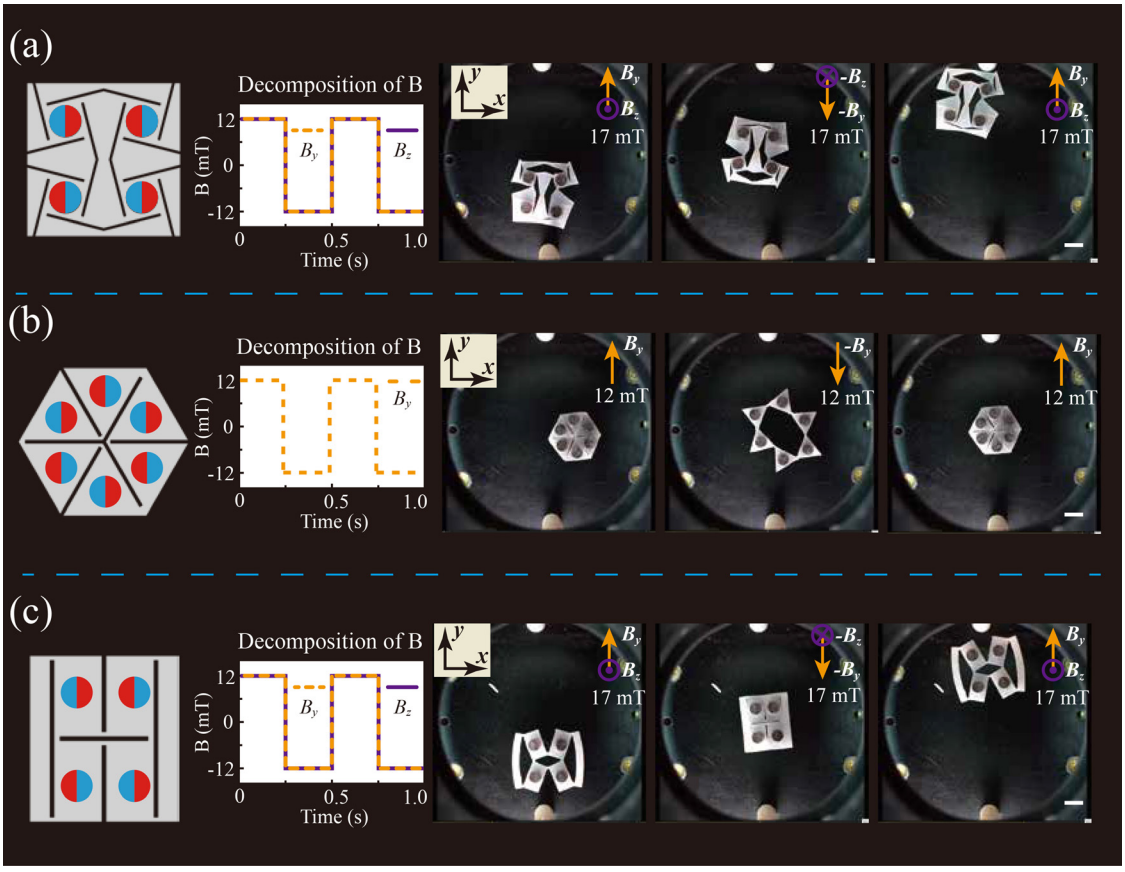

FIG. 11. Locomotion of kirigami soft robots with different cutting patterns. (a) The kirigami soft robot moves toward the +Y direction under a combined $\mathbf{B}_y$ and $\mathbf{B}_z$. (b) Triangular kirigaimi soft robot shows alternative expansion and contraction with large volume change. (c) The locomotion of a XS kirigami soft robot with a different aspect ratio. All the scale bars are 10 mm.

23 October 2023 12:40:25

Published under an exclusive license by AIP Publishing

we carefully aligned the marker to the desired directions. Another method to guarantee the magnetization direction is to change the geometry of the magnetic units from circular to square because the circle is symmetric to any line across the center. We have conducted experiments with kirigami soft robots with magnetic blocks. A XYS soft robot with four kirigami blocks was fabricated, and the locomotion under a combined square-wave $\mathbf{B}_y$ and $\mathbf{B}_z$ was tested (Fig. 12 and Movie 12). Results show that the kirigami soft robot with magnetic block walks more stable than those with magnetic disk. The trajectory is also almost straight.

B. Advantages of metamaterials in magnetic actuation

Magnetic actuation has superior advantages for fast and untethered actuation. Achieving programmable deformation often requires meticulous design of internal magnetization profile and external magnetic fields, imposing significant requirements on the magnetic robots' manufacturing and control. Metamaterial-based magnetic soft robots not only retain the advantages of immediate, remote, and reversible actuations found in hard-magnetic soft materials but also encompass the versatile attributes of metamaterials, such as shape morphing, auxetics and wave manipulation. Lattice and origami metamaterials have been widely combined with hard-magnetic soft materials to realize multifunctionality. For instance, integrating lattice metamaterials with hard-magnetic soft materials has enabled untethered revisable deformations, shape-locking,[49] and tunable stiffness and acoustic bandgaps.[46] Similarly, origami metamaterials have been combined with hard magnetic soft materials to realize multimodal deformation,[40,43] tunable physical properties for digital computing[42] and medicine delivery.[44]

In this study, we have combined the kirigami structure with hard-magnetic soft material to achieve stable locomotion, multifunctionality, and multimodal motions by virtue of the shape morphing and bistability of the kirigami structures. (i) Stable locomotion: Traditional soft robots rely on deformed configurations for motion, necessitating the precise design of internal magnetization profiles and external magnetic fields. Minor errors can lead to substantial deviations. In contrast, the kirigami soft robot employs mode transitions for locomotion, significantly reducing the dependence on internal magnetization profiles and external magnetic fields, thereby promoting stable movement. (ii) Multimodal motions: The kirigami structures may exhibit bistability by rational adjusting the geometric parameters, facilitating multimodal motions. We have incorporated bistability experiments to demonstrate that an amphibious kirigami soft robot can navigate on the ground and then transition to another stable state for underwater propulsion. (iii) Multifunctionality: The programmable 3D morphing also enables various functions, such as load-bearing and swimming via transitions between V and inverted V shapes and remote circuit through substantial out-of-plane bending.

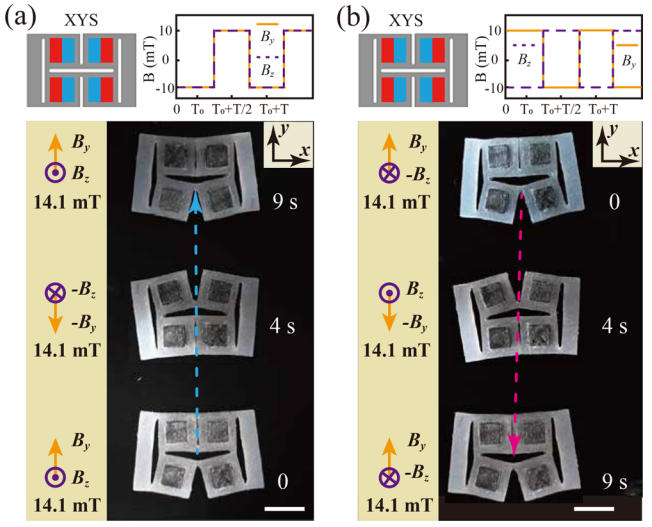

FIG. 12. The directional locomotion of the XYS kirigami soft robot with square magnetic units under a combined $\mathbf{B}_y$ and $\mathbf{B}_z$ with (a) zero phase difference and (b) π phase difference. All the scale bars are 10 mm.

IV. CONCLUSION

In this work, we develop an untethered kirigami soft robot consisting of slit perforated kirigami patterns with embedded hard-magnetic disks in each facet, which exhibits modularity, scalability and programmable locomotion. The hard-magnetic disks provide localized magnetic actuation, while the kirigami patterns provide large deformation and diverse functions. The kirigami patterns can induce both in-plane and out-of-plane shape transformations, significantly increasing the kinematics degree of freedom. The periodic arrangements of the kirigami patterns further enable easy combination of modular units. The kirigami structure also provides scalability, and kirigami soft robots with different sizes follow similar working principles.

The behaviors under static magnetic fields are studied systematically by combining experiments and FEM, which enables the exploration of the dynamic motions under oscillating magnetic fields. By controlling the magnetization arrays and the applied magnetic fields, we demonstrate multi-module soft robots with walking, crawling, flapping, and swing locomotion. Direction change is realized by the phase differences of magnetic fields, and asymmetric pattern enables circular motion. The soft robot also possesses superior active and passive environmental adaptability, such as crossing gaps, moving over various substrates and climbing slopes. In particular, we demonstrate a two-module soft robot with active adaptivity when encountering an obstacle, which changes the locomotion type and directions under the same applied magnetic field. We also demonstrate multifunctionalities, such as carrying large objects, acting as a remote circuit switch, removing obstacles on the slope and turning circularly. This work paves the way to design kirigami soft robots with programmable motions and multifunctionalities.

V. EXPERIMENTAL METHODS

A. Fabrications

The kirigami structure is made of silicone rubber (Smooth-On, Inc., Ecoflex 00–50). The shear modulus of the silicone rubber is ~50 kPa. The magnetic disks are fabricated by mixing 20 vol. % hard-magnetic particles (neodymium–iron–boron, NdFeB, ~ 5 μm in size) into the silicone rubber through a complete stirring. After being magnetized under an impulse field (~2 T), the magnetic disks possess an in-plane magnetization $\mathbf{M}$. For a typical assembly process of the single-module kirigami soft robot, four hard-magnetic disks with identical dimensions (diameter $d = 6$ mm, thickness $t = 2.5$ mm) are embedded into the center of each square with predefined orientations.

23 October 2023 12:40:25

Published under an exclusive license by AIP Publishing

The length L, width W, and thickness H are 26, 18, and 3 mm, respectively. A homemade DLP 3D printer is used to fabricate the miniature kirigami soft robots. The multi-module soft robots are made by molds with multiple unit patterns.

B. Finite element simulation

We conduct finite element analysis to investigate the deformation of kirigami soft robots using a commercially available finite-element software Abaqus 2021 (Dassault Systemes, France). The geometric patterns are the same as used in the experiments. Each kirigami soft robot model consists of two parts: silicone base and magnetic disks. The magnetic disks' sets are created by cell partition. A static step is created with the initial incrementation of 0.1 and the minimum incrementation of 1×10^{-6}. The Nlgeom is on for geometric nonlinearities. A general surface interaction with a linear contact stiffness 1×10^{8} for the normal surface behavior and a friction factor 0.3 for the tangential interaction are used for all exterior surfaces, while the interaction between the robots and motion platform is regarded as frictionless. The magnetic field is applied using a predefined field with four variables. The four variables are the three direction vectors and the magnitude of the applied magnetic fields.

A user-defined element subroutine developed by Zhao *et al.*[8,28] is used to predict the magnetically actuated deformation of the kirigami soft robots. This subroutine employs a neo-Hookean energy function with coupled Helmholtz potential to explicate the nonlinear deformation of magnetic structures. The unit direction vector and magnitude of the applied magnetic fields are defined as the initial input parameters. The materials' shear modulus and magnetization profiles are set according to the experimental material properties of the kirigami soft robots.

In the simulation, the gravity effect is considered as a body force with an acceleration of 9.8 m/s^2. The initial shear modulus $\mu = 100$ and 200 kPa are used for the silicone base and magnetic disks, respectively. The bulk modulus is chosen to be 1000 times the shear modulus to approximate the incompressibility. The magnetization intensity of magnetic disks is experimentally measured to be $M = 110$ kA/m. Owing to the magnetization of each magnetic disks is aligned with x-axis, the directional vector of magnetization profiles only switches between $+1$ and -1 in the x-direction. We employ a user-defined eight-node brick, linear elements in the FEA model. The actuation loading amplitude is defined to linearly increase from 0 to 1 during the timespan of magnetic actuation step. A code repository for the FEM simulation is available at https://github.com/Wang-s-Lab/kirigami-soft-robot-FEM.git.

SUPPLEMENTARY MATERIAL

See the supplementary material for the details of materials and methods, finite element analysis, magnetic actuation experiments and magnetic actuation setup. Programmable locomotion, adaptability, scalability, modularity, and multifunctionalities of kirigami soft robots are also demonstrated in the supplementary movies.

ACKNOWLEDGMENTS

D. Wang acknowledges support from Supported by the National Key Research and Development Program of China (No. 2022YFB4700900), the National Natural Science Foundation of China (Grant No. 52275025), the Interdisciplinary Program of Shanghai Jiao Tong University (Grant No. YG2021QN105), and the State Key Laboratory of Mechanical System and Vibration (Grant No. MSVZD202212).

AUTHOR DECLARATIONS

Conflict of Interest

The authors have no conflicts to disclose.

Author Contributions

J.W. and R.W. contributed equally to this work.

Jinqiang Wang: Conceptualization (lead); Investigation (equal); Validation (equal); Writing – original draft (lead). **Ruichen Wang:** Data curation (lead); Investigation (equal); Validation (equal). **Zixiao Zhu:** Data curation (equal); Software (lead). **Kun Zhou:** Supervision (equal); Visualization (equal). **Dong Wang:** Formal analysis (equal); Funding acquisition (lead); Writing – review & editing (lead).

DATA AVAILABILITY

The data that support the findings of this study are available from the corresponding author upon reasonable request.

REFERENCES

[1]C. Laschi, B. Mazzolai, and M. Cianchetti, "Soft robotics: Technologies and systems pushing the boundaries of robot abilities," Sci. Rob. **1**, eaah3690 (2016).
[2]D. Wang, J. Wang, Z. Shen, C. Jiang, J. Zou, L. Dong, N. X. Fang, and G. Gu, "Soft actuators and robots enabled by additive manufacturing," Annu. Rev. Control Rob. Auton. Syst. **6**, 31–63 (2023).
[3]M. Li, A. Pal, A. Aghakhani, A. Pena-Francesch, and M. Sitti, "Soft actuators for real-world applications," Nat. Rev. Mater. **7**, 235–249 (2022).
[4]D. Makarov, M. Melzer, D. Karnaushenko, and O. G. Schmidt, "Shapeable magnetoelectronics," Appl. Phys. Rev. **3**, 011101 (2016).
[5]C. S. X. Ng, M. W. M. Tan, C. Xu, Z. Yang, P. S. Lee, and G. Z. Lum, "Locomotion of miniature soft robots," Adv. Mater. **33**, 2003558 (2021).
[6]Q. Ge, Z. Chen, J. Cheng, B. Zhang, Y.-F. Zhang, H. Li, X. He, C. Yuan, J. Liu, S. Magdassi *et al.*, "3d printing of highly stretchable hydrogel with diverse UV curable polymers," Sci. Adv. **7**, eaba4261 (2021).
[7]G. Gu, J. Zou, R. Zhao, X. Zhao, and X. Zhu, "Soft wall-climbing robots," Sci. Rob. **3**, eaat2874 (2018).
[8]R. Zhao, Y. Kim, S. A. Chester, P. Sharma, and X. Zhao, "Mechanics of hard-magnetic soft materials," J. Mech. Phys. Solids **124**, 244–263 (2019).
[9]Y. Kim, J. van den Berg, and A. J. Crosby, "Autonomous snapping and jumping polymer gels," Nat. Mater. **20**, 1695–1701 (2021).
[10]Z. Li, N. V. Myung, and Y. Yin, "Light-powered soft steam engines for self-adaptive oscillation and biomimetic swimming," Sci. Rob. **6**, eabi4523 (2021).
[11]W. Pang, S. Xu, J. Wu, R. Bo, T. Jin, Y. Xiao, Z. Liu, F. Zhang, X. Cheng, K. Bai *et al.*, "A soft microrobot with highly deformable 3d actuators for climbing and transitioning complex surfaces," Proc. Natl. Acad. Sci. **119**, e2215028119 (2022).
[12]N. D. Thorat, S. A. Tofail, B. von Rechenberg, H. Townley, G. Brennan, C. Silien, H. M. Yadav, T. Steffen, and J. Bauer, "Physically stimulated nanotheranostics for next generation cancer therapy: Focus on magnetic and light stimulations," Appl. Phys. Rev. **6**, 041306 (2019).
[13]D. Jin, Q. Wang, K. F. Chan, N. Xia, H. Yang, Q. Wang, S. C. H. Yu, and L. Zhang, "Swarming self-adhesive microgels enabled aneurysm on-demand embolization in physiological blood flow," Sci. Adv. **9**, eadf9278 (2023).
[14]Y. Kim and X. Zhao, "Magnetic soft materials and robots," Chem. Rev. **122**, 5317–5364 (2022).
[15]A. Barbot, H. Tan, M. Power, F. Seichepine, and G.-Z. Yang, "Floating magnetic microrobots for fiber functionalization," Sci. Rob. **4**, eaax8336 (2019).
[16]Y. Kim, E. Genevriere, P. Harker, J. Choe, M. Balicki, R. W. Regenhardt, J. E. Vranic, A. A. Dmytriw, A. B. Patel, and X. Zhao, "Telerobotic neurovascular interventions with magnetic manipulation," Sci. Rob. **7**, eabg9907 (2022).

23 October 2023 12:40:25

Published under an exclusive license by AIP Publishing

[17]Z. Ren, W. Hu, X. Dong, and M. Sitti, "Multi-functional soft-bodied jellyfish-like swimming," Nat. Commun. **10**, 2703 (2019).
[18]M. Sun, C. Tian, L. Mao, X. Meng, X. Shen, B. Hao, X. Wang, H. Xie, and L. Zhang, "Reconfigurable magnetic slime robot: Deformation, adaptability, and multifunction," Adv. Funct. Mater. **32**, 2112508 (2022).
[19]T. Chen, M. Pauly, and P. M. Reis, "A reprogrammable mechanical metamaterial with stable memory," Nature **589**, 386–390 (2021).
[20]C. Hong, Z. Ren, C. Wang, M. Li, Y. Wu, D. Tang, W. Hu, and M. Sitti, "Magnetically actuated gearbox for the wireless control of millimeter-scale robots," Sci. Rob. **7**, eabo4401 (2022).
[21]S. Wu, Q. Ze, R. Zhang, N. Hu, Y. Cheng, F. Yang, and R. Zhao, "Symmetry-breaking actuation mechanism for soft robotics and active metamaterials," ACS Appl. Mater. Interfaces **11**, 41649–41658 (2019).
[22]R. D. Field, P. N. Anandakumaran, and S. K. Sia, "Soft medical microrobots: Design components and system integration," Appl. Phys. Rev. **6**, 041305 (2019).
[23]Y. Lee, F. Koehler, T. Dillon, G. Loke, Y. Kim, J. Marion, M.-J. Antonini, I. C. Garwood, A. Sahasrabudhe, K. Nagao *et al.*, "Magnetically actuated fiber-based soft robots," Adv. Mater. **35**, 2301916 (2023).
[24]C. Xu, Z. Yang, and G. Z. Lum, "Small-scale magnetic actuators with optimal six degrees-of-freedom," Adv. Mater. **33**, 2100170 (2021).
[25]W. Hu, G. Z. Lum, M. Mastrangeli, and M. Sitti, "Small-scale soft-bodied robot with multimodal locomotion," Nature **554**, 81–85 (2018).
[26]Q. Ze, X. Kuang, S. Wu, J. Wong, S. M. Montgomery, R. Zhang, J. M. Kovitz, F. Yang, H. J. Qi, and R. Zhao, "Magnetic shape memory polymers with integrated multifunctional shape manipulation," Adv. Mater. **32**, 1906657 (2020).
[27]Y. Dong, L. Wang, N. Xia, Z. Yang, C. Zhang, C. Pan, D. Jin, J. Zhang, C. Majidi, and L. Zhang, "Untethered small-scale magnetic soft robot with programmable magnetization and integrated multifunctional modules," Sci. Adv. **8**, eabn8932 (2022).
[28]Y. Kim, H. Yuk, R. Zhao, S. A. Chester, and X. Zhao, "Printing ferromagnetic domains for untethered fast-transforming soft materials," Nature **558**, 274–279 (2018).
[29]W. Chen, Z. Yan, and L. Wang, "On mechanics of functionally graded hard-magnetic soft beams," Int. J. Eng. Sci. **157**, 103391 (2020).
[30]G. Z. Lum, Z. Ye, X. Dong, H. Marvi, O. Erin, W. Hu, and M. Sitti, "Shape-programmable magnetic soft matter," Proc. Natl. Acad. Sci. **113**, E6007–E6015 (2016).
[31]D. Yan, A. Abbasi, and P. M. Reis, "A comprehensive framework for hard-magnetic beams: Reduced-order theory, 3d simulations, and experiments," Int. J. Solids Struct. **257**, 111319 (2022).
[32]H. Zhu, Y. Wang, Y. Ge, Y. Zhao, and C. Jiang, "Kirigami-inspired programmable soft magnetoresponsive actuators with versatile morphing modes," Adv. Sci. **9**, 2203711 (2022).
[33]C. Wang, Y. Wu, X. Dong, M. Armacki, and M. Sitti, "In situ sensing physiological properties of biological tissues using wireless miniature soft robots," Sci. Adv. **9**, eadg3988 (2023).
[34]X. Dong, G. Z. Lum, W. Hu, R. Zhang, Z. Ren, P. R. Onck, and M. Sitti, "Bioinspired cilia arrays with programmable nonreciprocal motion and metachronal coordination," Sci. Adv. **6**, eabc9323 (2020).
[35]C. Ma, S. Wu, Q. Ze, X. Kuang, R. Zhang, H. J. Qi, and R. Zhao, "Magnetic multimaterial printing for multimodal shape transformation with tunable properties and shiftable mechanical behaviors," ACS Appl. Mater. Interfaces **13**, 12639–12648 (2020).
[36]T. Xu, J. Zhang, M. Salehizadeh, O. Onaizah, and E. Diller, "Millimeter-scale flexible robots with programmable three-dimensional magnetization and motions," Sci. Rob. **4**, eaav4494 (2019).
[37]X. Yang, W. Shang, H. Lu, Y. Liu, L. Yang, R. Tan, X. Wu, and Y. Shen, "An agglutinate magnetic spray transforms inanimate objects into millirobots for biomedical applications," Sci. Rob. **5**, eabc8191 (2020).
[38]Y. Alapan, A. C. Karacakol, S. N. Guzelhan, I. Isik, and M. Sitti, "Reprogrammable shape morphing of magnetic soft machines," Sci. Adv. **6**, eabc6414 (2020).
[39]H. Deng, K. Sattari, Y. Xie, P. Liao, Z. Yan, and J. Lin, "Laser reprogramming magnetic anisotropy in soft composites for reconfigurable 3d shaping," Nat. Commun. **11**, 6325 (2020).
[40]S. Yi, L. Wang, Z. Chen, J. Wang, X. Song, P. Liu, Y. Zhang, Q. Luo, L. Peng, Z. Wu *et al.*, "High-throughput fabrication of soft magneto-origami machines," Nat. Commun. **13**, 4177 (2022).
[41]R. H. Soon, Z. Yin, M. A. Dogan, N. O. Dogan, M. E. Tiryaki, A. C. Karacakol, A. Aydin, P. Esmaeili-Dokht, and M. Sitti, "Pangolin-inspired untethered magnetic robot for on-demand biomedical heating applications," Nat. Commun. **14**, 3320 (2023).
[42]L. S. Novelino, Q. Ze, S. Wu, G. H. Paulino, and R. Zhao, "Untethered control of functional origami microrobots with distributed actuation," Proc. Natl. Acad. Sci. **117**, 24096–24101 (2020).
[43]S. Wu, Q. Ze, J. Dai, N. Udipi, G. H. Paulino, and R. Zhao, "Stretchable origami robotic arm with omnidirectional bending and twisting," Proc. Natl. Acad. Sci. **118**, e2110023118 (2021).
[44]Q. Ze, S. Wu, J. Dai, S. Leanza, G. Ikeda, P. C. Yang, G. Iaccarino, and R. R. Zhao, "Spinning-enabled wireless amphibious origami millirobot," Nat. Commun. **13**, 3118 (2022).
[45]Q. Ze, S. Wu, J. Nishikawa, J. Dai, Y. Sun, S. Leanza, C. Zemelka, L. S. Novelino, G. H. Paulino, and R. R. Zhao, "Soft robotic origami crawler," Sci. Adv. **8**, eabm7834 (2022).
[46]S. M. Montgomery, S. Wu, X. Kuang, C. D. Armstrong, C. Zemelka, Q. Ze, R. Zhang, R. Zhao, and H. J. Qi, "Magneto-mechanical metamaterials with widely tunable mechanical properties and acoustic bandgaps," Adv. Funct. Mater. **31**, 2005319 (2021).
[47]S. Roh, L. B. Okello, N. Golbasi, J. P. Hankwitz, J. A.-C. Liu, J. B. Tracy, and O. D. Velev, "3d-printed silicone soft architectures with programmed magneto-capillary reconfiguration," Adv. Mater. Technol. **4**, 1800528 (2019).
[48]J. Zhang, Z. Ren, W. Hu, R. H. Soon, I. C. Yasa, Z. Liu, and M. Sitti, "Voxelated three-dimensional miniature magnetic soft machines via multimaterial heterogeneous assembly," Sci. Rob. **6**, eabf0112 (2021).
[49]B. Zou, Z. Liang, D. Zhong, Z. Cui, K. Xiao, S. Shao, and J. Ju, "Magneto-thermomechanically reprogrammable mechanical metamaterials," Adv. Mater. **35**, 2207349 (2023).
[50]T. van Manen, S. Janbaz, M. Ganjian, and A. A. Zadpoor, "Kirigami-enabled self-folding origami," Mater. Today **32**, 59–67 (2020).
[51]Z. Zhai, L. Wu, and H. Jiang, "Mechanical metamaterials based on origami and kirigami," Appl. Phys. Rev. **8**, 041319 (2021).
[52]Y. Hong, Y. Chi, S. Wu, Y. Li, Y. Zhu, and J. Yin, "Boundary curvature guided programmable shape-morphing kirigami sheets," Nat. Commun. **13**, 530 (2022).
[53]Y. Yang, K. Vella, and D. P. Holmes, "Grasping with kirigami shells," Sci. Rob. **6**, eabd6426 (2021).
[54]A. Rafsanjani and D. Pasini, "Bistable auxetic mechanical metamaterials inspired by ancient geometric motifs," Extreme Mech. Lett. **9**, 291–296 (2016).

23 October 2023 12:40:25

Published under an exclusive license by AIP Publishing